

Technical Notes

TECHNICAL NOTES are short manuscripts describing new developments or important results of a preliminary nature. These Notes cannot exceed 6 manuscript pages and 3 figures; a page of text may be substituted for a figure and vice versa. After informal review by the editors, they may be published within a few months of the date of receipt. Style requirements are the same as for regular contributions (see inside back cover).

Shock Wave Focusing in a Log-Spiral Duct

O. Inoue,* N. Takahashi,† and K. Takayama‡
Tohoku University, Sendai, Japan

Introduction

A LOGARITHMIC spiral (log-spiral) duct was contrived by Milton¹ as an effective tool to produce an extremely high pressure and temperature by focusing an initially plane shock wave. According to the ray shock theory,² no triple-point (or reflected shock wave) is expected to form in a log-spiral duct until the implosion is completed. In fact, no reflected shock wave was seen in shadowgraphs taken by Milton.¹ On the other hand, after implosion Milton observed an intense vortex in the flow behind the reflected shock wave. Then a question arises: What is the mechanism of the vortex formation? Milton suggests that a triple point may appear in a flowfield very close to the focus. The appearance of the triple point might be related to the formation of the vortex. At present, however, it seems pretty difficult to analyze experimentally the detailed flowfield close to the focus. The purpose of this study is to simulate numerically the shock wave focusing process in a log-spiral duct and to clarify the mechanism of the formation of a vortex behind the reflected shock wave after implosion.

Numerical Method

A two-dimensional, log-spiral duct adopted in this study is presented in Fig. 1. The duct is assumed to be symmetric with respect to the plane BO. The duct is designed such that an initially plane shock wave focuses at a point O. The configuration of the duct is determined by the characteristic length L and the characteristic angle χ and is described as follows¹:

$$r = R \exp\left(\frac{\chi - \phi}{\tan \chi}\right) \quad (1)$$

where $R = L/\cos \chi$. Upstream of point A, the wall is assumed to be straight. In the following, lengths are nondimensionalized by L . The two-dimensional Euler equations were solved:

$$\frac{\partial Q}{\partial t} + \frac{\partial E}{\partial x} + \frac{\partial F}{\partial y} = 0 \quad (2)$$

where x and y are the coordinates, and t is the time. The symbols Q , E , and F are flux vectors and are expressed as follows:

$$Q = \begin{pmatrix} \rho \\ \rho u \\ \rho v \\ e \end{pmatrix}, \quad E = \begin{pmatrix} \rho u \\ \rho u^2 + p \\ \rho uv \\ (e + p)u \end{pmatrix}, \quad F = \begin{pmatrix} \rho v \\ \rho vu \\ \rho v^2 + p \\ (e + p)v \end{pmatrix} \quad (3)$$

where u and v are the velocity components in x and y directions, respectively, ρ the density, and e the total energy per unit volume. The pressure p is given as $p = (\gamma - 1)[e - \rho(u^2 + v^2)/2]$, where γ is the specific heat ratio and is fixed to be 1.4 in this study. A MUSCL total variation diminishing (TVD) finite volume method with flux-vector splitting³ was used. For time integration, the Runge-Kutta scheme was adopted. Computational accuracy is of the second order both in time and

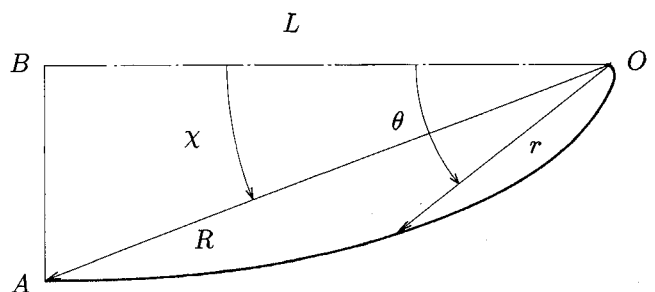


Fig. 1 Log-spiral duct.

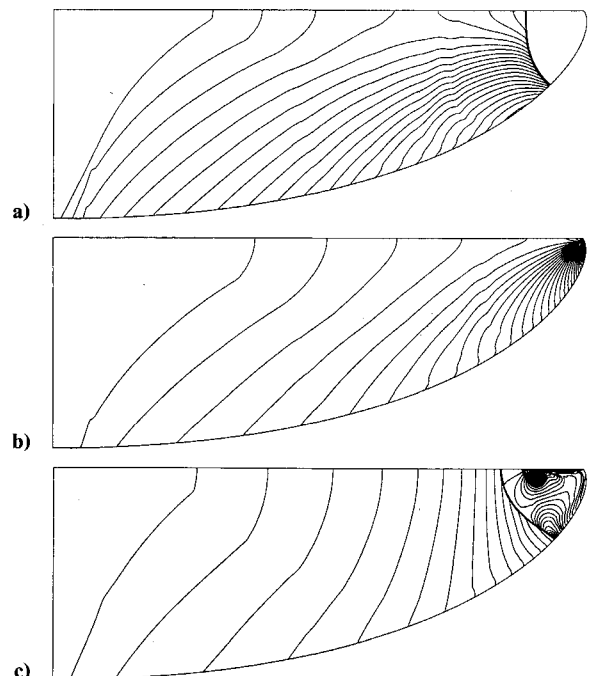


Fig. 2 Focusing process in a log-spiral duct; isopycnics, $M_0 = 2.3$, $\chi = 22.5$ deg: a) $t = 0.3854$ (before focusing), b) $t = 0.4303$ (just before focusing), and c) $t = 0.5165$ (after focusing).

Received May 19, 1992; accepted for publication Nov. 7, 1992. Copyright © 1992 by O. Inoue, N. Takahashi, and K. Takayama. Published by the American Institute of Aeronautics and Astronautics, Inc., with permission.

*Associate Professor, Institute of Fluid Science. Member AIAA.

†Graduate Student, Department of Mechanical Engineering; currently, Engineer, Fuji Heavy Industries, Ltd., Kaname Minami 1-1-11, Utsunomiya 320, Japan.

‡Professor, Institute of Fluid Science. Member AIAA.

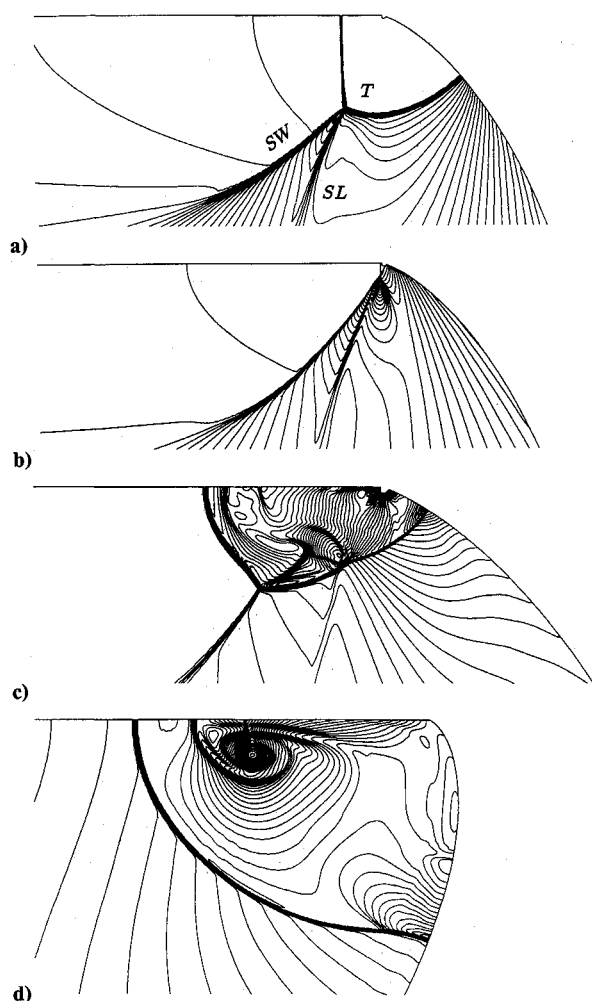
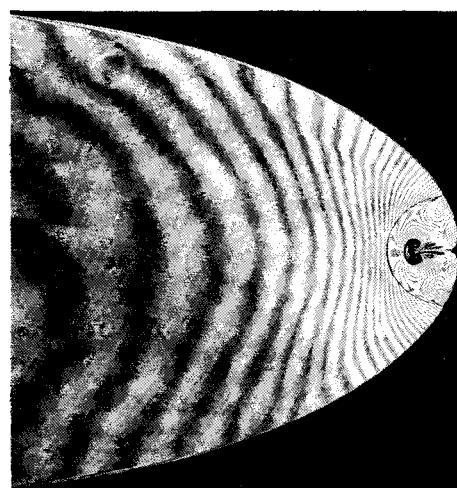
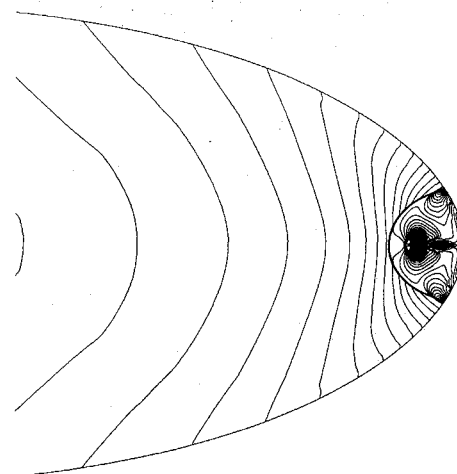


Fig. 3 Detailed mechanism of vortex formation; isopycnics, $M_0 = 2.3$, $\chi = 22.5$ deg: a) $t = 0.4303$ (before focusing, $m = 50$), b) $t = 0.4308$ (just before focusing $m = 100$), c) $t = 0.4313$ (after focusing, $m = 100$), and d) $t = 0.4654$ (after focusing, $m = 6.25$).



a)



b)

Fig. 4 Comparison with experiment; isopycnics: a) experiment, $M_0 = 2.3$; b) computation, $M_0 = 2.3$, $t = 0.5165$.

space. The number of grids are 32,000 (1600 along the log-spiral wall by 200 perpendicular to the wall).

Results and Discussion

The shock wave focusing process was simulated for several different configurations of a log-spiral duct by changing χ or equivalently the Mach number M_0 of the incident shock wave. However, qualitative features of the focusing process were not dependent on the configurations. A typical example of focusing is shown in Fig. 2. As the flow is symmetric with respect to the plane BO in Fig. 1, only the lower half is presented in Fig. 2 (and also in Fig. 3). No reflected shock wave seems to form until the implosion is completed (Figs. 2a and 2b). After implosion, on the other hand, a single reflected shock moves outward and a vortex can be seen behind the reflected shock (Fig. 2c). The flow feature shown in Fig. 2 is close to that observed by Milton.¹ The detailed structures in the flowfield near the focus are presented in Fig. 3 for the same case as in Fig. 2. Each view of the flowfield shown in Fig. 3 is magnified, respectively, and the magnification rate is given by the symbol m . An initially plane shock wave moves at a constant speed along the symmetric plane (BO), whereas it accelerates along the log-spiral wall. As a result, the shock wave bends (Fig. 2a), and with increasing distance the pressure gradient along the shock wave becomes larger. With a sufficiently large pressure gradient, a second shock wave (SW in Fig. 3a) is formed, and a slip line (SL in Fig. 3a) is emanated from the triple point (T). The second shock wave and the slip line survive through the

implosion (Figs. 3b and 3c). After the implosion, a reflected shock wave moves outward and interacts with the second shock wave and the slip line, respectively. These two interactions produce, respectively, new slip lines behind the reflected shock wave (Fig. 3c). Vorticity produced by the two slip lines merges into a single vortex (Fig. 3d). It may be interesting to see that a new shock wave is formed in the vortex. A comparison of a calculated flowfield with experimental observation by holographic interferometric photography, sufficiently after the implosion is completed, is presented in Fig. 4. As readily seen from Fig. 4, the two flowfields are very close to each other. Therefore, we may say that the present results simulate the focusing process very well.

The configuration of a log-spiral duct is determined such that the characteristics of the ray shock theory are centered at a focusing point (O in Fig. 1) and do not intersect with each other at any other point. Therefore, a triple point is not expected to appear before the implosion. The computational results in Fig. 3, as well as the results for other configurations examined in this study, however, show that the triple point does not appear before the implosion. Careful examination of the computational results indicates that the appearance of the triple point may not be related to the intersection of the characteristics. A possible reason for the failure of the ray shock theory to predict the appearance of the triple point may be due to the assumption of quasi-one-dimensionality adopted in characteristic rules. That is, immediately before the implosion, variation of flow quantities along the shock wave such as pressure and density gradients is very large (Fig. 3a), and thus the assumption of quasi-one-dimensionality does not hold. Here, it should be mentioned that the appearance of the triple

point before the implosion is confined within the range of a few percent of the characteristic length L from a focusing point. Therefore, we may say that the ray shock theory² gives a reasonable approximation to the flowfield so far as the flowfield far from the focus is concerned.

Acknowledgments

The first author expresses his sincere thanks to Asako Inoue for her continuous encouragement. The authors express their gratitude to B. E. Milton, University of New South Wales, Australia, for his kind advice and suggestions. Thanks are also due to K. Sawada, Institute of Fluid Science, Tohoku University, for his assistance in this study.

References

- ¹Milton, B. E., "The Focusing of Shock Waves in Two-Dimensional and Axi-Symmetric Ducts," *Proceedings of the International Workshop on Shock Wave Focusing*, edited by K. Takayama, Inst. of Fluid Science, Tohoku Univ., Sendai, Japan, 1989, pp. 155-191.
- ²Milton, B. E., "Mach Reflection Using Ray-Shock Theory," *AIAA Journal*, Vol. 13, No. 11, 1975, pp. 1531-1533.
- ³Leer, B. V., "Flux-Vector Splitting for the Euler Equations," *Proceedings of the 8th International Conference on Numerical Methods in Fluid Dynamics*, Lecture Notes in Physics, Vol. 170, Springer-Verlag, 1982, pp. 507-512.

Introduction

THE flow separation aft of a blunt-based axisymmetric body at zero angle of attack creates an axisymmetric wake that is the most complex part of the flowfield. An axisymmetric wake consists of a near-wake region and a far-wake region. The near-wake region exists just after the body base, creating a recirculation region covered by the free-shear layer.

Delery and Siriex¹ and Delery and Lacau² outlined the axisymmetric wake physics based on earlier investigations. Merz et al.³ investigated the effect of Mach number on the turbulent near-wake of a cylindrical blunt-based body over the entire subsonic Mach number range. Merz et al.⁴ also experimentally investigated the near wake of an axisymmetric semi-elliptical afterbody. Atli⁵ performed some hot-wire measurements to investigate the wakes of four complex bodies of revolution at zero angle of attack. Despite these and other works, new investigations are necessary for more information on the problem because of its fundamental and practical importance. New data may also be useful for comparison with computational predictions of the flowfield.

In the present work the wakes of three axisymmetric missile-type bodies with different afterbody geometry at zero angle of attack and at a low subsonic velocity were studied by using a constant temperature hot-wire anemometer. Mean velocity and turbulence measurements, both along and across the wake, were performed. Turbulence was considered as the time-averaged rms fluctuating velocities. Vortex shedding and instability in the free-shear layer were not treated.

Wakes of Three Axisymmetric Bodies at Zero Angle of Attack

Özlem İlday,* Hayri Acar,† M. Kubilay Elbay,‡
and Veysel Atli§
Istanbul Technical University, Istanbul, Turkey

Nomenclature

C_D	= drag coefficient
d	= maximum diameter of the model
l	= total length of the model
Re_d	= Reynolds number based on maximum body diameter, $U_\infty d / \nu$
r	= radial distance from the wake centerline
r_b	= r position where $\bar{U}_d = \frac{1}{2}(\bar{U}_d)_{\max}$
U_∞	= freestream velocity
\bar{U}	= mean velocity in the x direction
\bar{U}_d	= velocity defect, $\bar{U}_{\max} - \bar{U}$
$\sqrt{(u')^2}$	= rms velocity fluctuations in the x direction
u_0	= $\sqrt{(u')^2} / U_\infty$
u_1	= $\sqrt{(u'_{CL})^2} / U_\infty$
u_2	= $\sqrt{(u'_{CL})^2} / \bar{U}_{CL} $
x	= distance from the base of the model in the freestream direction
x_{sp}	= length of the recirculation region

Subscript

CL = centerline of the wake

Models and Experimental Technique

The models shown in Fig. 1 have the same fineness ratio, $l/d = 16.4$, with the same tangent-ogive nose and cylindrical main body. The first model has a flared afterbody with a neck, the second one a blunt base, and the third one a truncated conical afterbody (boat-tail). The surfaces of the models were smooth.

All of the tests were conducted at zero angle of attack in an open-circuit, low-speed wind tunnel with a closed test section of $50 \times 50 \times 200$ cm. The freestream velocity U_∞ was 10 m/s ($M_\infty \approx 0.03$) with the freestream turbulence intensity $\sqrt{(u')^2} / U_\infty = 0.3\%$. The Reynolds number Re_d based on maximum body diameter was 2×10^4 . A hot-wire anemometer system of DISA (55M) was used with a personal computer and an Analog/Digital converter of Data Acquisition 380 Validyne. The models were supported from one side by two thin circular stings 5 mm in diameter. The support of the hot-wire probe was placed perpendicular to the model symmetry axis and to the model supports to minimize the effects of the supports. Blockage area ratio was less than 0.3% so that no correction for blockage effects has been made. The positional accuracy of the probe traverse was ± 0.1 mm, and the accuracy of the hot-wire anemometer outputs for mean velocity and fluctuations is about ± 0.1 and ± 0.002 m/s, respectively.

The outputs of a hot-wire anemometer do not indicate the flow direction; in other words, the mean velocity output of the

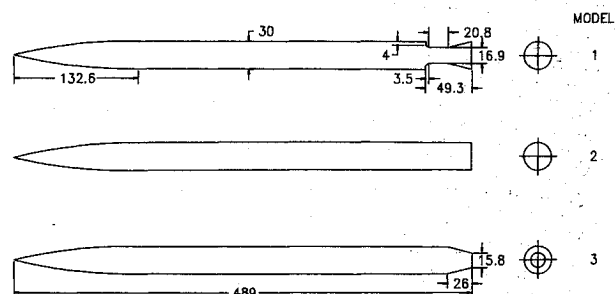


Fig. 1 Model geometries (dimensions in mm).

Received Oct. 21, 1991; revision received Sept. 6, 1992; accepted for publication Sept. 15, 1992. Copyright © 1992 by the American Institute of Aeronautics and Astronautics, Inc. All rights reserved.

*Research Assistant, Aeronautical Engineer, Faculty of Aeronautics and Astronautics, 80626 Maslak.

†Research Assistant, Aeronautical Engineer, Faculty of Aeronautics and Astronautics, 80626 Maslak.

‡Research Assistant, Aeronautical Engineer, Faculty of Aeronautics and Astronautics, 80626 Maslak.

§Associate Professor, Faculty of Aeronautics and Astronautics, 80626 Maslak.